# A dual-axis, high-sensitivity atomic magnetometer*

Rujie Li(李茹杰)†, Wei Quan(全伟)‡, Wenfeng Fan(范文峰), Li Xing (邢力), Zhuo Wang(王卓), Yueyang Zhai(翟跃阳), and Jiancheng Fang(房建成)

*School of Instrument Science and Opto-electronics Engineering, Beihang University, Beijing* 100191, *China*

(Received 16 July 2017; revised manuscript received 25 August 2017; published online 20 October 2017)

Atomic magnetometer (AM) operated in a spin-exchange relaxation-free (SERF) regime features superior sensitivity and non-cryogenic operation, and thus is competitive with the best superconducting quantum interference devices. Previously, SERF AM with fT/Hz$^{1/2}$ level sensitivity commonly acted as a single-axis sensor. Here we demonstrate a dual-axis SERF AM capable of simultaneously and independently detecting *x*- and *y*-field components with a sensitivity of 20 fT/Hz$^{1/2}$. As there is no necessity to worry about the cross-talk effects arising from field modulations, the dual-axis scheme proposed here is of particular interest to AM array and hence the biomagnetic applications.

**Keywords:** optically pumped magnetometers, multi-axis field measurements, high-sensitivity field measurements, polarized atoms

**PACS:** 07.55.Ge, 07.07.Df, 42.81.Pa **DOI:** 10.1088/1674-1056/26/12/120702

## 1. Introduction

It has been approximately sixty years since the appearance of the atomic magnetometer (AM) pioneered by Dehmelt, Bell and Bloom.[1,2] Utilizing the Larmor precession of an ensemble of electronic or nuclear spins, cell-based AMs obtain the ability to sense magnetic fields.[3–5] High-sensitivity AMs are valuable in various applications, covering studies of nuclear magnetic resonance (NMR) signals,[6] searches for permanent electric dipole moments (EDM),[7] magnetic induction tomography (MIT),[8] measurements of magnetoencephalography (MEG),[9] and magnetocardiography (MCG).[10] With sensitivities of a few fT/Hz$^{1/2}$, the traditional superconducting quantum interference devices (SQUIDs) operated at cryogenic temperatures have been used for the most demanding applications. However, the advances in AMs, especially the development of spin-exchange relaxation-free (SERF) AM, have enabled the alkali-metal magnetometer to achieve sensitivity surpassing that of SQUIDs in both a low-frequency mode[11] and a radio-frequency (RF) mode.[12] Besides, AMs offer other advantages, such as compact package, low-power dissipation and without the need for complex cryogenic equipment. Recently, AMs have been used to explore some of the applications previously dominated by SQUIDs.[9,13–15]

The SERF AMs, whose sensitivities have reached sub-fT/Hz$^{1/2}$ and established the new sensitivity record for AMs in the low-frequency range,[11] commonly acted as a single-axis sensor by using the traditional orthogonal pump-probe configuration,[15–17] *z*-field modulation mode,[18] single elliptically polarized-beam design[19] or parallel (two-color) pump-probe scheme.[9,20] In most of the cases, single-axis AMs are just oriented along a certain direction to detect the projected components of the fields. However, multi-axis AM will provide a favorable experimental condition for the vector measurements, and thus improve the signal quality and reduce the orientation difficulty of the sensor head.[21] Utilizing the modulation techniques,[22] Seltzer *et al.* reported a three-axis SERF AM with a sensitivity of 1 pT/Hz$^{1/2}$, dominated by the fluctuations of the ambient magnetic field, in an unshielded environment. However, the modulated fields therein will introduce cross-talk effects when AM array is used.[23] By alternating the pumping beam direction with a time-divided switcher, Kim *et al.* described a multi-channel AM with the ability to measure two orthogonal fields in a shielded environment.[24] Recently, Morales *et al.* presents a proof of concept study which demonstrates for the first time the possibility to record MCG signals with $^4$He vector optically-pumped magnetometers (OPM) in a magnetically shielded room.[25] Via theoretical analysis on the feasibility of two orthogonal probe beams, which extended the conventional pump-probe configuration, here we demonstrate a dual-axis SERF AM capable of simultaneously and independently detecting *x*- and *y*-field components with a sensitivity of 20 fT/Hz$^{1/2}$ in a shielded environment. The dual-axis, high-sensitivity AM can be of interest to the investigations on NMR and EDM where vector-field measurements are generally required. As there is no necessity to worry about the cross-talk effects due to field modulations, the dual-axis scheme proposed here is especially useful for AM array and hence the MEG or MCG applications.[24] Dual-axis

*Project supported by the National Natural Science Foundation of China (Grant Nos. 61227902, 61673041, and 61374210), the National Key R & D Program of China (Grant No. 2016YFB0501601), and the Academic Excellence Foundation of Beihang University (BUAA) for PhD Students.

†Corresponding author. E-mail: lirujie@buaa.edu.cn

‡Corresponding author. E-mail: quanwei@buaa.edu.cn

© 2017 Chinese Physical Society and IOP Publishing Ltd 

gyroscopes can reduce the complexity and the cost of Inertial Measurement Unit (IMU), thus the dual-axis probe scheme proposed here can advance the atomic spin gyroscope (ASG) pioneered by Kornack *et al.* by providing an ideal tool for practical realization of two-axis SERF gyroscope predicted in our previous work.[26,27]

The steady-state transverse responses of optically pumped magnetometer are described as[28]

$$P_x^{\mathrm{e}} = P_0^{\mathrm{e}} \frac{\beta_y + \beta_x\beta_z}{1+\left(\beta_x{}^2+\beta_y{}^2+\beta_z{}^2\right)}, \tag{1}$$

$$P_y^{\mathrm{e}} = P_0^{\mathrm{e}} \frac{-\beta_x + \beta_y\beta_z}{1+\left(\beta_x{}^2+\beta_y{}^2+\beta_z{}^2\right)}, \tag{2}$$

where $\boldsymbol{\beta} = \gamma^e \boldsymbol{B}/R_{\mathrm{tot}}^{\mathrm{e}}$, $\gamma^e$ is the gyromagnetic ratio of the free electronic spins, $\boldsymbol{B}$ is the external magnetic field vector, $R_{\mathrm{tot}}^{\mathrm{e}}$ is sum of the pumping rate $R_{\mathrm{p}}$ and the relaxation rate $R_{\mathrm{rel}}$ sensed by the electronic spins,[16] the equilibrium polarization $P_0^{\mathrm{e}}$ along the $z$ axis (pump beam direction) is determined by the balance of $R_{\mathrm{p}}$ and $R_{\mathrm{rel}}$, $P_x^{\mathrm{e}}$ and $P_y^{\mathrm{e}}$ are the projected components of $P_0^{\mathrm{e}}$ along $x$ and $y$ axes. If the ambient field $\boldsymbol{B}$ is weak enough (typically, less than 0.5 nT), such that $|\beta|^2 \ll 1$, $|\beta_x\beta_z| \ll |\beta_y|$, and $|\beta_y\beta_z| \ll |\beta_x|$, equations (1) and (2) are simplified, given by

$$P_x^{\mathrm{e}} \approx \frac{P_0^{\mathrm{e}}\gamma^e}{R_{\mathrm{tot}}^{\mathrm{e}}} B_y, \tag{3}$$

$$P_y^{\mathrm{e}} \approx -\frac{P_0^{\mathrm{e}}\gamma^e}{R_{\mathrm{tot}}^{\mathrm{e}}} B_x, \tag{4}$$

where the AM is operated in the SERF regime. Equations (3) and (4) indicate that $P_x^{\mathrm{e}}$ and $P_y^{\mathrm{e}}$, which can be detected by two separate probe beams propagated along $x$ and $y$ axes, are independently sensitive to $B_y$ and $B_x$, respectively. This is also our initial motivation to design a dual-axis AM with two orthogonal probe beams. Note that a weak $B_z$ is necessary to keep $|\beta_x\beta_z| \ll |\beta_y|$ and $|\beta_y\beta_z| \ll |\beta_x|$, and a non-zero $B_z$ will lead to a slight cross-talk effect between the two axes due to the term $\beta_x\beta_z$ in Eq. (1) and the term $\beta_y\beta_z$ in Eq. (2). It should also be addressed that the cross-talk terms just provide a powerful tool for zeroing the residual fields.[22] In our case, $z$ component of the field can be easily nulled with an accuracy of better than 0.05 nT.

## 2. Experimental apparatus

The optical layout of the dual-axis SERF AM is illustrated in Fig. 1, while the sensor head is shown in Fig. 2. At its heart is a spherical vapor cell with a diameter of 10 mm. The cell is made from aluminosilicate glass and contains a mixture of K and Rb alkali metals in natural abundance. 50 Torr (1 Torr = $1.33322\times10^2$ Pa) of $N_2$ quenching gas and 1.9 amagat of $^4$He buffer gas also fill the cell during the cell fabrication process. The cell is heated to 180 °C by running ac current through a resistor mounted on the exterior of the oven. Using the laser absorption spectroscopy,[29] the density ratio of K to Rb atoms is estimated to be 1:87. The heating apparatus is mounted inside a 3-layer $\mu$-metal magnetic shield with cylindrical profiles in order to operate near zero magnetic field and screen out environmental magnetic noise. In addition to further reduce the residual fields, three pairs of orthogonal coils are also used to provide the calibration signals. The pump beam, formed by an external cavity diode laser (ECDL) and turned to the K $D_1$ resonance line at 770.1 nm, is introduced into the system by a fiber feedthrough. The cell is illuminated by the pump beam with an intensity of 10.2 mW/cm$^2$, thus the K atoms are polarized along the $z$ direction. Rb atoms are polarized via the rapid spin-exchange collisions between K and Rb atoms.[30] Due to the smaller optical depth of K atoms in the hybrid scheme, the polarization of alkali-metal atoms are much more homogenous.

The probe beam is emitted from a distributed feedback (DFB) laser diode held in the head of prototype AM. It is detuned by about 0.3 nm to the red side of Rb $D_2$ resonance line to increase the AM signals. A photoelastic modulator (PEM) with a resonance frequency of $f_{\mathrm{mod}} = 84$ kHz and a modulation amplitude of $\alpha = 0.4$ rad is used to modulate the polarization of probe beam in order to separate the weak rotation signal from $1/f$ noise. The probe beam is initially polarized by a linear polarizer (LP). The PEM, the quarter waveplate, the analyzer are oriented at 45°, 0°, and 90° with respect to the transmission axis of the polarizer, respectively. The probe beam becomes elliptically polarized light, whose fast axis also varies with a frequency of $f$, after passing through the PEM. A quarter waveplate is generally used to further adjust the polarization state of the elliptically polarized light in order to obtain a simplified first-harmonic signal sensed by the detector after the analyzer, $I \approx I_0\alpha\theta\sin(2\pi ft)$, where $I_0$ is the intensity of the incident light and $\theta$ is the rotation angle induced by the polarized atoms. Note that the probe beam enters the cell with elliptically polarized state and the rotation angle $\theta$ can be treated as the rotation of linear components of the elliptically polarized beam. Aimed at modulating the two probe beams in our dual-axis AM with one PEM, here we place the PEM ahead of the vapor cell and then the modulated beam is split into two branches by a beam splitter. A theoretical analysis on the PEM-based probe system has been reported.[31] As shown in Fig. 1, Ch1 and Ch2 probe beams continuously detect the projection of the Rb spin polarization along $x$ and $y$ axis through optical rotation of the linearly polarized light. Utilizing a lock-in amplifier with a low-pass filter of 200 Hz cut-frequency, we could extract the field-induced rotations signals. The output signals of dual-axis SERF AM are digitized with a sampling rate of 1 kHz using a 24-bit data acquisition system.

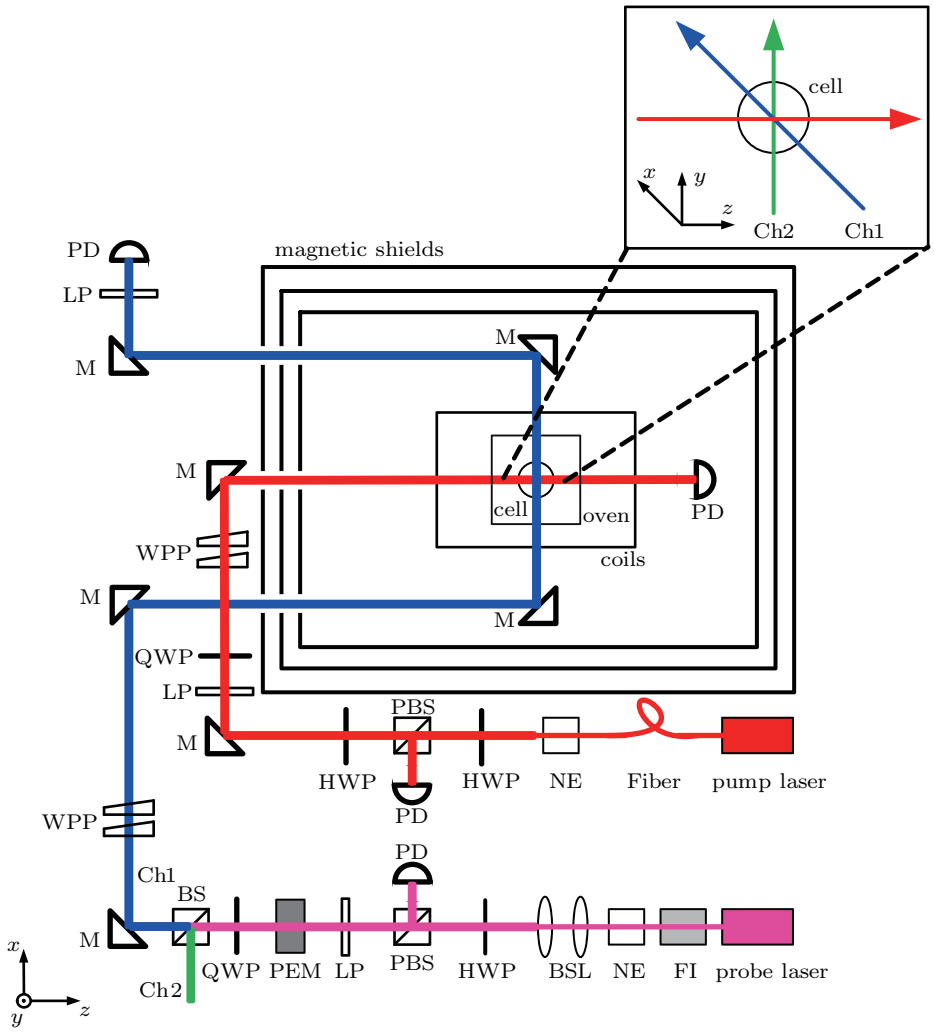



**Fig. 1.** (color online) The optical layout of the dual-axis SERF AM. FI: Faraday isolator, NE: noise eater, BSL: beam shaping lenses, HWP: half waveplate, PBS: polarizing beam splitter, PD: silicon photodiode, BS: beam splitter, PEM: photoelastic modulator, LP: linear polarizer, QWP: quarter waveplate, M: reflection mirror, WPP: wedge prism pairs. The pump beam is circularly polarized in order to polarize the atoms. The probe beam splits into two branches by the BS and the laser intensity of each branch is about 2.1 mW/cm$^2$. As the optical layout of Ch2 probe beam is the same as Ch1 except the orthogonal propagation direction shown in the top inset, the subsequent components after BS in Ch2 have been dropped. Three laser beams (one pump beam and two probe beams) meet at the cell center, and they are perpendicular to each other. The relaxation rates due to the two off-resonant probe beams are negligible compared to the pumping effect arising from the resonant pump laser.

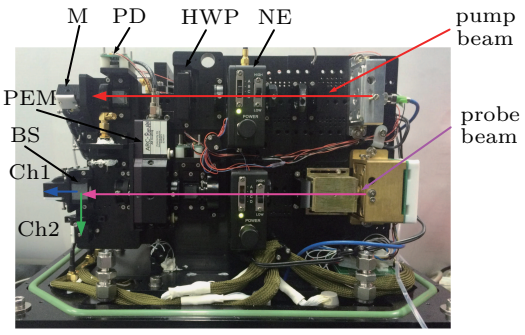



**Fig. 2.** (color online) Side view of the dual-axis SERF AM. It has an outer dimension of 350 mm×325 mm×250 mm and most of the elements therein are home-built. The probe laser (located at the beginning of the pink arrow) has been assembled in the sensor head and it splits into Ch1 (blue arrow) and Ch2 (green arrow) probe beams, which output the response of Ch1 AM and Ch2 AM. The pump laser is introduced into the system by a fiber feedthrough (not shown), and fiber collimator held at the beginning of the red arrow output the pump beam. Most of the elements are made of non-magnetic and non-metallic materials to minimize the residual field and field inhomogeneities around the vapor cell. Details of the optical layout are illustrated in Fig. 1.

## 3. Measurement results

An oscillating field $B = B'\cos(\omega t)\hat{y}$ is generally applied to calibrate the AM. This field can be decomposed into two counter-propagating rotating fields, written as

$$B = \frac{\mathrm{i}B'}{2}\left(\mathrm{e}^{\mathrm{i}\omega t} + \mathrm{e}^{-\mathrm{i}\omega t}\right). \tag{5}$$

Among them, the component $B = \mathrm{i}B'\,\mathrm{e}^{\mathrm{i}\omega t}/2$ induces a precession projected on the $x$ axis, expressed as

$$P_x^{\mathrm{e}} = \frac{P_0^{\mathrm{e}}\gamma^{\mathrm{e}}B'}{2q(P_0^{\mathrm{e}})}\frac{\cos(\omega t + \phi)}{\sqrt{(\Delta\omega)^2 + (\omega - \omega_0)^2}}, \tag{6}$$

which is centered at frequency $\omega_0$ with half width at half maximum (HWHM) $\Delta\omega = R_{\mathrm{tot}}^{\mathrm{e}}/q(P_0^{\mathrm{e}})$, $q(P_0^{\mathrm{e}})$ is the nuclear slowing-down factor, and $\omega_0$ is the resonance frequency due to the residual fields. A phase shift $\phi$, which depends on the relaxation rate of the atoms as well as the frequency of the fields, occurs compared to input signal.

The magnetic field responses of the dual-axis AM to oscillating fields are depicted in Fig. 3. To distinguish the responses from dual channels, two oscillating magnetic fields with different frequencies (11 Hz for $B_y$, 25 Hz for $B_x$) are fed into Ch1 and Ch2 AMs. RMS amplitudes of both calibration signals are 40 pT. Due to the higher frequency of $B_x$, the absolute phase shift of Ch2 is greater than that of Ch1.

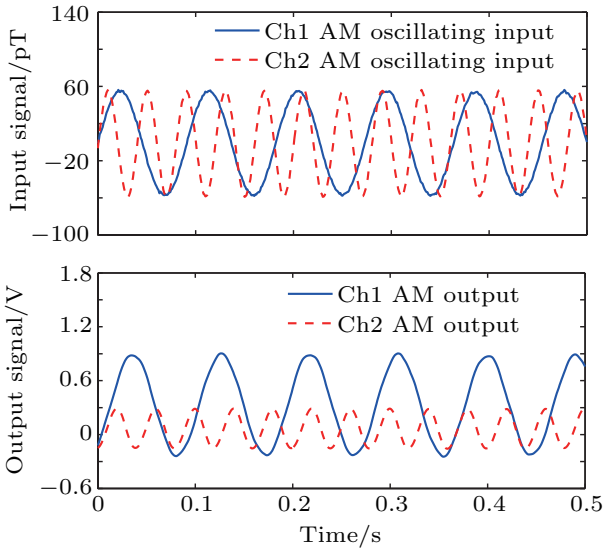



**Fig. 3.** (color online) Time-varying input (top) and output (bottom) signals of the dual-axis AM. The initial phases of the input signals are zeroed, while those of output signals are shifted by −52.1 deg and −82.6 deg derived from the corresponding fitting curves.

Figure 4 shows the AM frequency response. The fitting curves based on Eq. (6) yielded that the bandwidths are 9.5 Hz and 9.3 Hz for Ch1 and Ch2 AMs. The different response strength between Ch1 and Ch2 AMs at the same frequency is due to the imbalance of the probe beam intensities. By employing the feedback technique or using a higher-intensity pump beam, we could increase the bandwidths.[32]

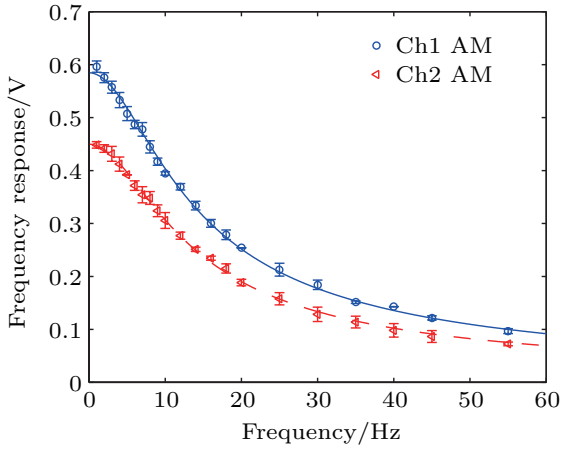



**Fig. 4.** (color online) Frequency response of the dual-axis AM. Two magnetic fields, whose frequency varies from 1 Hz to 55 Hz, are applied to $B_y$ and $B_x$ in order to test the bandwidth of Ch1 and Ch2 AMs.

By dividing the power spectral density (PSD) of 100-s output signals by the frequency response mentioned above, we obtain the normalized sensitivity spectrums of the dual-axis AM, as shown in Fig. 5. The peaks with frequency of 11 Hz in Ch1 AM and 25 Hz in Ch2 AM represent the calibration signals, which are referred to the oscillating fields shown in Fig. 3. Both Ch1 and Ch2 AMs feature a sensitivity of 20 fT/Hz$^{1/2}$ in the band from 8 Hz to 60 Hz. Also shown are the traces of probe systems, which give a noise floor of 6 fT/Hz$^{1/2}$. It is three times lower than the sensitivity of our prototype AM. The innermost layer of shields with an inner radius of $r = 48$ mm and a thickness of $t = 2$ mm corresponds to a Johnson noise of 24 fT/Hz$^{1/2}$ in theory,[33,34] and thus is the dominant noise source in our measurement. By removing the shields and placing the sensor head in a magnetically shielded room (MSR),[23,35] we could overcome this limitation. The signal with a frequency of 25 Hz (11 Hz) displayed in Ch1 (Ch2) AM is due to the slight cross-talk effect from the other channel. This phenomenon what we suspect is due to the non-orthogonality of the three-axis coils, or the residual magnetic field and light shift along the $z$ direction.[36,37] Note the coupling is more than two orders of magnitude weaker than the calibration signals and 25 times smaller than the 50-Hz disturbance from the power supply lines. These perturbations can be suppressed by use of notch filters. Additionally, the undesired interferences at 19 Hz and 31 Hz in AMs and the probe systems are the result of the air conditioning fans located inside the roof of our laboratory. The much stronger disturbance in Ch1 also implies the noise is mainly in the $y$ direction. This imperfection can be reduced in a gradiometry arrangement,[8,11] which is in progress. The response of the dual-axis AM to the field offset in $B_x$ and $B_y$ is presented in Fig. 6. Both Ch1 (blue line) and Ch2 AMs (red dashed line) show a linear measurement range of about 1 nT. It implies a weak field environment, such as a good shielded room or a proper field-controlling technique, is necessary for the normal operation of the SERF AM.

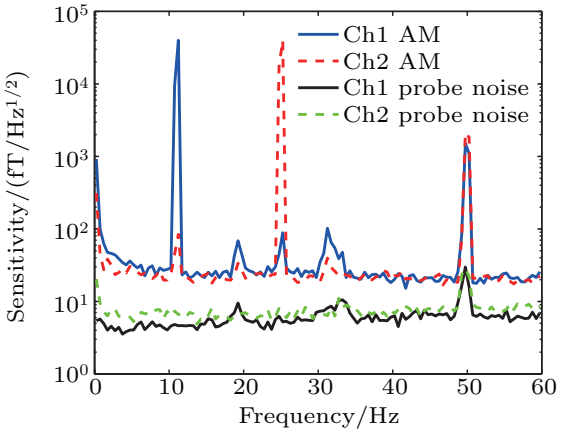



**Fig. 5.** (color online) Sensitivity of the dual-axis AM and noise of the probe beams. Both Ch1 (blue line) and Ch2 (red dashed line) AMs feature a magnetic field sensitivity of 20 fT/Hz$^{1/2}$. By turning off the pump beam and the oscillation fields, we obtain the spectrums of the probe beams (black line for Ch1 and green dashed line for Ch2), which give a noise floor of about 6 fT/Hz$^{1/2}$.

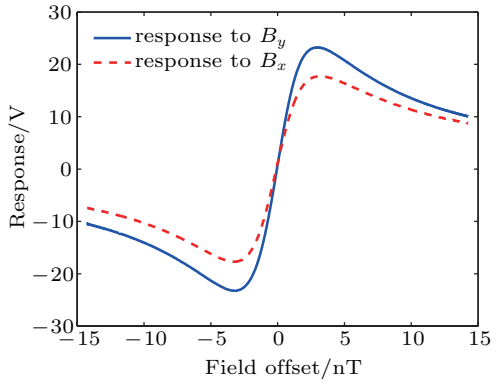



**Fig. 6.** (color online) The response of the dual-axis AM to the field offset in $B_x$ and $B_y$. Both Ch1 (blue line) and Ch2 AMs (red dashed line) show a linear measurement range of about 1 nT.

## 4. Conclusion and future work

Via theoretical analysis on the physical model of the AM, the feasibility of dual-axis measurements has been proposed. Utilizing an artful arrangement of two orthogonal probe beams, we have demonstrated a dual-axis SERF AM capable of simultaneously and independently detecting $x$- and $y$-field components with a sensitivity of 20 fT/Hz$^{1/2}$. This research advances the time-divided magnetometer reported by Kim *et al.*[24] As there is no necessity to worry about the cross-talk effects arising from field modulations,[22] the dual-axis scheme proposed here is of particular interest to AM array,[23,24] as well as the corresponding potential MEG or MCG applications. While considerable progress has been made to reject the unwanted interference by sophisticated hard- and software solutions, instead of the magnetic shields, we believe the efforts aiming at the magnetometer with multi-axis capacity and low cost are also necessary. Further investigations on the AM operated in an unshielded environment will contribute to the dissemination of AM-based biomagnetic applications. Lacking the need for complex and expensive cryogenic equipment in SQUIDs, SERF AM also features a compact package and low-power dissipation. The optics with microelectromechanical systems (MEMS) technology and the techniques first developed for chip-scale atomic clocks support a high-performance, millimeter-scale microfabricated dual-axis AM.[38–40]

Even though a dual-axis, high-sensitivity AM has been reported here, we also identify further improvements. A better sensitivity can be obtained by removing the magnetic shields and placing the sensor head in MSR.[23] Utilizing the technique of real-time closed-loop feedback, we could improve the AM bandwidth and further suppress the cross-talk effect.[32] As Cs has a higher saturated vapor pressure than other alkali metals, Cs-based AM might be specially attractive to applications requiring lower temperature.[16]

## References


[1] Dehmelt H G 1957 *Phys. Rev.* **105** 1924
[2] Bell W E and Bloom A L 1957 *Phys. Rev.* **107** 1559
[3] Bloom A L 1962 *Appl. Opt.* **1** 61
[4] Grujić Z D, Koss P A, Bison G and Weis A 2015 *Eur. Phys. J. D* **69** 135
[5] Fu J Q, Du P C, Zhou Q and Wang R Q 2016 *Chin. Phys. B* **25** 010302
[6] Xu S, Yashchuk V V, Donaldson M H, Rochester S M, Budker D and Pines A 2006 *Proc. Natl. Acad. Sci. USA* **103** 12668
[7] Baker C A, Doyle D D, Geltenbort P, Green K, van der Grinten M G D, Harris P G, Iaydjiev P, Ivanov S N, May D J R, Pendlebury J M, Richardson J D, Shiers D and Smith K F 2006 *Phys. Rev. Lett.* **97** 131801
[8] Marmugi L and Renzoni F 2016 *Sci. Rep.* **6** 23962
[9] Johnson C, Schwindt P D D and Weisend M 2010 *Appl. Phys. Lett.* **97** 243703
[10] Groeger S, Bison G, Knowles P E, Wynands R and Weis A 2006 *Sensors Actuat. A: Phys.* **129** 1
[11] Dang H B, Maloof A C and Romalis M V 2010 *Appl. Phys. Lett.* **97** 151110
[12] Keder D A, Prescott D W, Conovaloff A W and Sauer K L 2014 *AIP Adv.* **4** 127159
[13] Yashchuk V V, Granwehr J, Kimball D F, Rochester S M, Trabesinger A H, Urban J T, Budker D and Pines A 2004 *Phys. Rev. Lett.* **93** 160801
[14] Savukov I M and Romalis M V 2005 *Phys. Rev. Lett.* **94** 123001
[15] Wyllie R, Kauer M, Smetana G S, Wakai R T and Walker T G 2012 *Phys. Med. Biol.* **57** 2619
[16] Fang J, Li R, Duan L, Chen Y and Quan W 2015 *Rev. Sci. Instrum.* **86** 073116
[17] Wang M L, Wang M B, Zhang G Y and Zhao K F 2016 *Chin. Phys. B* **25** 060701
[18] Li Z, Wakai R T and Walker T G 2006 *Appl. Phys. Lett.* **89** 134105
[19] Shah V and Romalis M V 2009 *Phys. Rev. A* **80** 013416
[20] Li Y, Wang Z, Jin S, Yuan J and Luo H 2017 *Sci. Rep.* **7** 43066
[21] Koch H 2004 *J. Electrocardiol.* **37** 117
[22] Seltzer S J and Romalis M V 2004 *Appl. Phys. Lett.* **85** 4804
[23] Wyllie R, Kauer M, Wakai R T and Walker T G 2012 *Opt. Lett.* **37** 2247
[24] Kim K, Begus S, Xia H, Lee S K, Jazbinsek V, Trontelj Z and Romalis M V 2014 *Neuroimage* **89** 143
[25] Morales S, Corsi M C, Fourcault W, Bertrand F, Cauffet G, Gobbo C, Alcouffe F, Lenouvel F, Le Prado M, Berger F, Vanzetto G and Labyt E 2017 *Phys. Med. Biol.* **62** 7267
[26] Kornack T W, Ghosh R K, Romalis M V 2005 *Phys. Rev. Lett.* **95** 230801
[27] Li R, Fan W, Jiang L, Duan L, Quan W and Fang J 2016 *Phys. Rev. A* **94** 032109
[28] Seltzer, S J 2008 "Developments in Alkali-Metal Atomic Magnetometry", Ph. D. Dissertation (USA: Princeton University)
[29] Li R, Li Y, Jiang L, Quan W, Ding M and Fang J 2016 *Eur. Phys. J. D* **70** 139
[30] Babcock E, Nelson I, Kadlecek S, Driehuys B, Anderson L W, Hersman F W and Walker T G 2003 *Phys. Rev. Lett.* **91** 123003
[31] Duan L, Fang J, Li R, Jiang L, Ding M and Wang W 2015 *Opt. Express* **23** 32481
[32] Lee H J, Shim J H, Moon H S and Kim K 2014 *Opt. Express* **22** 19887
[33] Kornack T W, Smullin S J, Lee S K and Romalis M V 2007 *Appl. Phys. Lett.* **90** 223501
[34] Mateos I, Patton B, Zhivun E, Budker D, Wurm D and Ramos-Castro J 2015 *Sensors Actuat. A: Phys.* **224** 147
[35] Altarev I, Fierlinger P, Lins T, Marino M G, Nießen B, Petzoldt G, Reisner M, Stuiber S, Sturm M, Taggart Singh J, Taubenheim B, Rohrer H K and Schläpfer U 2015 *J. Appl. Phys.* **117** 233903
[36] Sulai I A, Wyllie R, Kauer M, Smetana G S, Wakai R T and Walker T G 2013 *Opt. Lett.* **38** 974
[37] Schultze V, Schillig B, Ijsselsteijn R, Scholtes T, Woetzel S and Stolz R 2017 *Sensors* **17** 561
[38] Knappe S, Shah V, Schwindt P D D, Hollberg L, Kitching J, Liew L A and Moreland J 2004 *Appl. Phys. Lett.* **85** 1460
[39] Eklund E J, Shkel A M, Knappe S, Donley E and Kitching J 2008 *Sensors Actuat. A: Phys.* **143** 175
[40] Deng K, Chen X and Wang Z 2011 *Opt. Lett.* **36** 1740